


Experimental phase transition mapping for hydrogen above 300 K up to 300 GPaChang-Sheng Zha ^{1,*}, Hanyu Liu,² Zhongwu Wang,³ and William A. Bassett⁴¹*Earth and Planets Laboratory, Carnegie Institution of Washington, 5241 Broad Branch Road NW, Washington DC 20015, USA*²*International Center for Computational Method & Software, and State Key Lab of Superhard Materials, College of Physics, Jilin University, Changchun 130012, People's Republic of China*³*Cornell High Energy Synchrotron Source (CHESS), Cornell University, Ithaca, New York 14853, USA*⁴*Department of Earth and Atmospheric Sciences, Cornell University, Ithaca, New York 14853, USA*

(Received 8 March 2023; accepted 10 July 2023; published 14 August 2023)

We report a phase diagram mapping for solid hydrogen based on several thousands of Raman spectroscopic data points obtained at simultaneous high-pressure and -temperature (PT) experiments. Information about phase behavior in the range of 300 K up to the melting line and 0–300 GPa for hydrogen has remained almost unknown to date; therefore, revealing it is very desirable. A network analysis of the isothermal and isobaric dependencies for various Raman modes has been used; discontinuities in these dependencies, plus the mode appearance/disappearance provide evidence for phase transitions. These transition data show self-consistency and have been used to outline possible phase boundaries for hydrogen in this PT region. Evidence we found shows hydrogen may experience a gradual molecular dissociation process before its metallization.

DOI: [10.1103/PhysRevResearch.5.033100](https://doi.org/10.1103/PhysRevResearch.5.033100)**I. INTRODUCTION**

Precise prediction of hydrogen phase change including metallic transition has been a long-standing effort because of the enormous zero-point energy (ZPE) for this lightest element. The large quantum fluctuation strongly affects the theoretical calculations such that there has been continuous improvement in the predicted transition pressure for metallic hydrogen [1–4]. Experimental methods are still the only reliable ways to study the phase diagram of the hydrogen system. In 2017, we successfully used the externally heated diamond anvil cell (DAC) in conjunction with micro-Raman scattering system for studying the melting curve of hydrogen. [5] High-quality Raman spectra for intramolecular vibration (vibron) and lattice modes can be obtained up to 300 GPa at 295–900 K, where the disappearance of lattice modes can be used as the melting criterion at certain pressure-temperature points to define the melting curve. The Raman spectra we obtained, except for melting, surely contain valuable information concerning potential solid-solid phase transitions in the portion below the melting lines. However, work for revealing this information was not pursued at that time. In the last several decades, only four solid hydrogen phases have been confirmed, mostly by Raman scattering and IR absorption experiments conducted below or at room temperature. [1,6–16] A large portion of the phase diagram above room temperature

up to the melting curve still remains unknown. Only a few experiments with limited PT data points above 300 K have been tried, and the reported results are far from convincing and not self-consistent. [17]

As is well known, the activity of the Raman mode depends on the lattice symmetry; therefore, phase transition induced by changes of pressure and/or temperature should cause Raman modes to appear, disappear, or undergo discrete frequency and peak-width shifting. Two phase mapping pathways can be used to find the physical discontinuities: method 1, by increasing pressure at fixed temperature (isothermal), or method 2, by increasing temperature at fixed pressure (isobaric). Discontinuities in either of these two dependencies are considered to be the phase transition points at the phase boundaries. However, heating hydrogen above room temperature up to ~1000 K under very high pressure causes big technical challenges for the experiment, because the hot dense hydrogen has a strong tendency to break diamond and damage the gasket materials. This, on the one hand, requires the smoothest and shortest possible heating durations, which can greatly reduce the possibility of chemical reaction between hydrogen and diamond or gasket. On the other hand, changing the force loading to the DAC during heating often introduces a high rate of diamond/gasket failure. This means pressure adjustment at constant high temperatures is not preferred. Doing the sample heating without touching the DAC (i.e., constant force loading) favorably meets the two requirements above and can greatly improve the sample's chance of surviving the higher temperatures even at very high pressures. For this reason, we chose the constant-force-loading heating procedure for each run.

In a 2017 study, the melting transition featured a unique criterion, namely, the disappearance of lattice Raman modes and melting measurements made by recording the *in situ*

*Author to whom correspondence should be addressed: czha@carnegiescience.edu

Published by the American Physical Society under the terms of the [Creative Commons Attribution 4.0 International](https://creativecommons.org/licenses/by/4.0/) license. Further distribution of this work must maintain attribution to the author(s) and the published article's title, journal citation, and DOI.

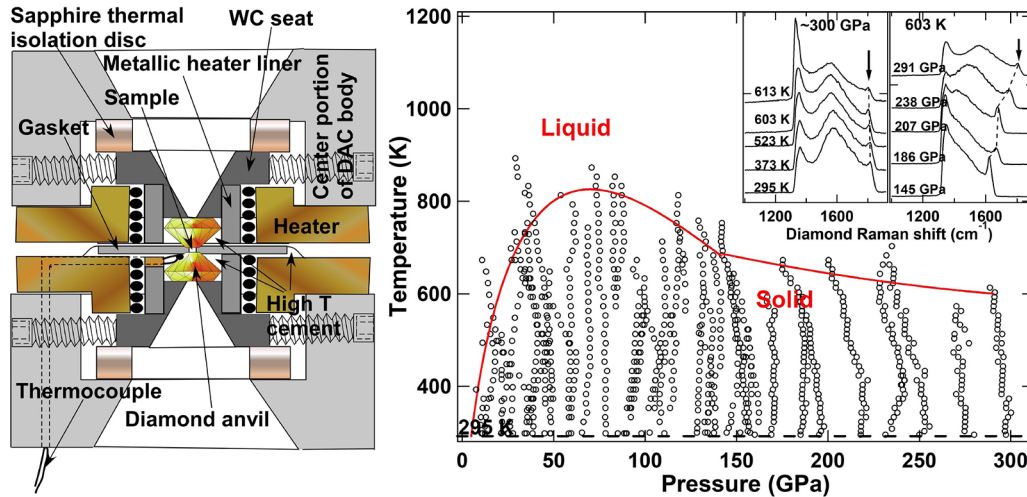


FIG. 1. Left: The interior of a specially designed, symmetric, diamond anvil cell (DAC). Two identical resistive heaters closely surrounding the anvils and gasket ensure a very rapid and homogeneous heating for the sample. Two sapphire disks were used to offer effective thermal isolation between hot diamond seats and DAC body. The hottest portion was also designed to be far enough away from the piston-cylinder fitting surface which is out of the range of this drawing. This arrangement permits making smaller tolerance between the sliding piston-cylinder mechanisms that deliver much stable force to the anvils. This, in turn, allows the DAC to reach higher pressures at higher sample temperatures while minimizing the pressure variation during the heating. Right: Plot of pressure-temperature distribution of partial experimental data points (circles) and melting lines (red lines). Inset: Diamond Raman spectra showing sharp peaks in the high-frequency portion of the spectrum, indicate that the spectra come from a soft solid hydrogen sample. It has been the criterion for using this kind of spectrum as a reliable source for *in situ* pressure determination (see Fig. S2 in the Supplemental Material (SM) [18] for details).

measured pressure-temperature values at the disappearing points. At the same time, the spectra of the intramolecular vibration Raman mode of hydrogen (vibron ν_1) were always obtained at each specific temperature increment. Discontinuous changes in this mode induced by pressure or temperature were widely used for the indication of hydrogen phase transitions previously. However, different from the unique criterion of melting, solid-solid phase transitions could be more complicated either by mode appearance or disappearance, while in many cases they might only be manifested with a discontinuous shift of mode frequency. Unfortunately, there is always the chance that heating may cause spurious random pressure changes even though the DAC's force-loading mechanical parts are not touched. These may result from the complex effects of thermal expansion of DAC parts and deformation of the metal gasket. These changes can also produce Raman frequency shifts, so during a constant-force-loading heating run, frequency shifts from both temperature and pressure change may be mixed and can be impossible to distinguish. This is the reason why the raw frequency-temperature data obtained in a single constant-force-loading heating run cannot be used for recognizing the solid-solid phase transition directly. We need to distinguish these mixed observations to find the pure effects resulting from pressure and temperature, respectively. In order to accomplish that, a large number of different PT data points, obtained in the heating runs with dense temperature and pressure increments, are needed to organize an isothermal and isobaric vibron frequency network.

II. EXPERIMENT AND RESULTS

During an almost decade long period, hundreds of runs of high-PT experiments on hydrogen were conducted. [5]

Approximately 3500 Raman spectra from more than 1000 PT data points were obtained. To successfully obtain high-quality Raman spectra at such large PT extreme conditions, a specially designed symmetric DAC with improved external heating techniques was used. The left side of Fig. 1 shows the internal portion of the high-temperature DAC. The key structural improvement (as described in figure caption) not only ensures a uniform temperature distribution across the sample, but also offers very rapid heating rates that allow us to quickly achieve thermal stabilization at each temperature increment. The resulting shorter heating time for the whole run reduces the chance for chemical reactions between hydrogen and parts of the DAC. The thermocouple junction is cemented adjacent to the sample providing the most reliable sample temperature determination. For each heating run, a fresh high-pressure sample was loaded, the sample was compressed to a desired pressure at room temperature, and it was allowed to become stabilized with the final pressure checked by the hydrogen vibron frequency at room temperature as published previously [14]. A preset stepwise heating run under constant force loading was performed.

In situ pressure determination during heating is critical for constructing an accurate phase diagram at very high pressures. Pressure measurements for most portions of the diagram use the diamond-Raman-frequency method as shown in the Supplemental Material (SM) [18]. A sharp peak feature in the high-frequency portion of the broadened diamond Raman spectrum (Fig. 1, inset) is always obtained even at very high pressure and temperature. It is the indication of relatively uniform pressure distribution available only when a soft sample like hydrogen or helium is contained. [9,14,19,20] The peak position is sensitive to pressure in the heating run, and the uncertainty for reading it is $\pm 2 \text{ cm}^{-1}$. Spectra have demonstrated

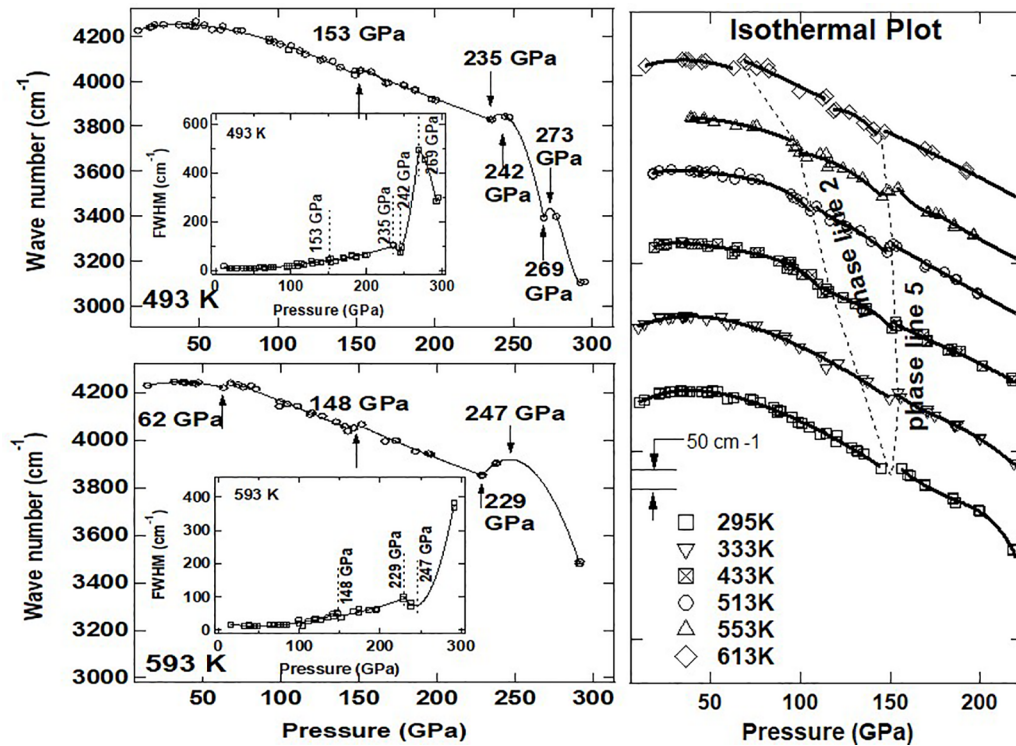


FIG. 2. Left: Plots showing the pressure dependence of vibron ν_1 frequency and peak width (insets) at 493 and 593 K. Symbols (circles and squares) are data points; each coming from individual heating experimental runs. Small arrows mark kinks in vibron frequencies indicating possible phase transitions; vertical dashed lines mark kinks in FWHM of vibron ν_1 peaks. Solid lines within each kink-free interval are polynomial fitting curves for that pressure range that offer a possibility for calculating frequency at desired pressures and constructing isobaric plots. Right: Different shaped symbols (listed) are used for a collection of six different isothermal plots of vibron ν_1 frequency illustrating how features like kinks offer reliable evidence of phase transitions when lines like the dashed ones can be used to connect them.

that the intensity of this peak is proportional to the hydrogen sample volume; [14] a weaker peak corresponds to a smaller sample volume and the disappearance of a peak most likely indicates the pressure condition is strongly affected by some source other than hydrogen, leading to very high pressure uncertainty. For this reason, the diamond Raman spectra without this sharp peak were never used for the pressure determination. This criterion could be important for determining the real hydrogen pressure required by the study under such high PT conditions, in which sample abundance strongly affects the pressure gradients. The *in situ* pressure values for each data point at high temperature are obtained based on two parts of the pressure measurement. The starting pressure at room temperature is always determined using the averaged pressure dependence of the hydrogen vibron frequency obtained previously [14] which is reasonably consistent with various recent studies (Fig. S3 of the SM [18]); it is then corrected with pressure variation caused by heating for obtaining the pressures at high T . The pressure variations during heating are the difference calculated from Akahama's scale [20], by inputting measured room-temperature diamond Raman shift and those measured at each temperature increment, respectively. The frequency-temperature shift at room pressure for diamond Raman is taken into account with assumption of no pressure cross effect for its thermal shift. [21] The details of the pressure determination method are shown in Fig. S2 of the SM [18] and validated by *in situ* high-PT x-ray diffraction and Raman scattering at a synchrotron radiation facility as

mentioned in the Supplemental Material of Ref. [5]. We note that, although the diamond Raman pressure scale may not be a precise enough method, the important thing is keeping the pressure measuring method and results as consistent as possible between different investigations for this research project. The method we used here for determining the pressure of hydrogen at high temperature might be the most reasonable way available at the moment.

Because a single constant-force-loaded heating run does not offer exclusive isobaric phase transition information as discussed above, a systematic analysis for a large amount of data has to be used to distinguish evidence of real phase changes from any spurious signals. The first step is to create the isothermal pressure dependency of the vibron frequencies, using the same temperature points obtained from each of the constant-force-loaded heating runs. Taken all together, those runs yield a network covering a wide PT range up to ~ 300 GPa and ~ 900 K. Figure 2 (left) shows examples of isothermal pressure dependencies of vibron ν_1 frequency and peak width at two different temperatures. The vibron frequency at 493 K initially decreases with pressure above ~ 30 GPa, and displays an abrupt slope increase around 235 GPa followed by other steeper slope changes at higher pressures. These observed slope changes also change with temperature as shown at 593 K. The abrupt increase of peak width [full width at half maximum (FWHM)] as shown in the insets of Fig. 2 (left) can be attributed to the structural anharmonicity variation caused by phase transformation, providing

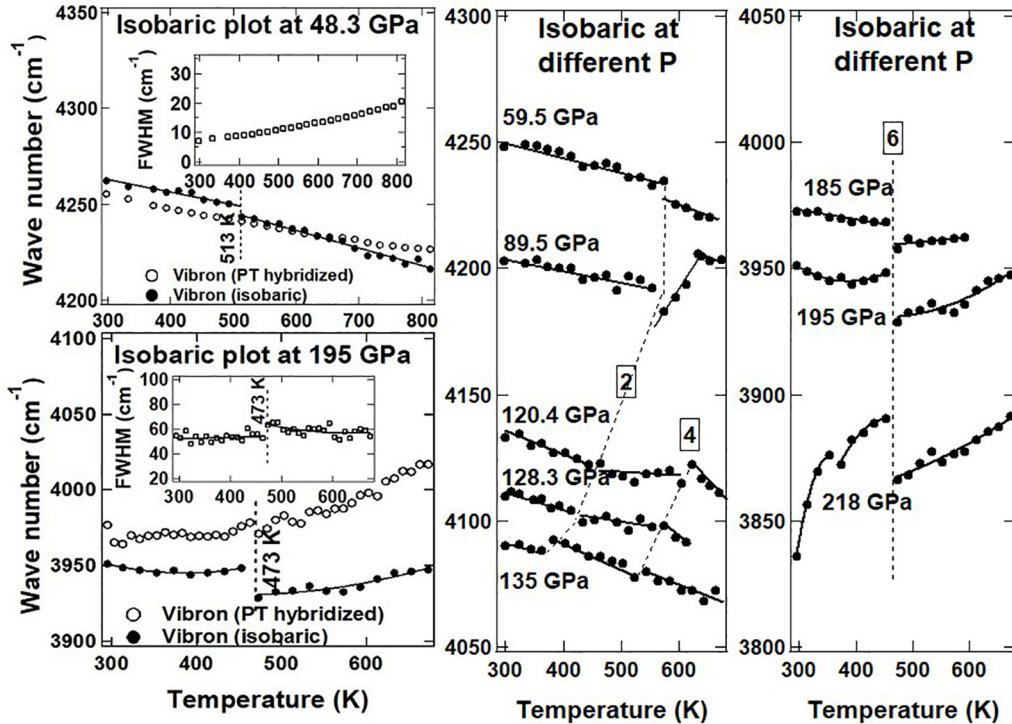


FIG. 3. Left: Isobaric frequency-temperature plots for vibron ν_1 in two different pressure runs. The frequencies measured during the constant-force-loaded heating runs are hybridized results contributed by both changes of pressure and temperature (open circles), whereas the real isobaric vibron frequencies (solid circles) are obtained from the fitted isothermal curves at different temperatures as shown in Figs. 2 and S4 of the SM [18]. Symbols are the data points; solid lines are for guiding the eye. Plots for peak width (FWHM) changing with temperature are also shown in the inset. Middle and right: List plot for isobaric temperature dependence of vibron ν_1 frequency at eight pressures. Discontinuities appearing systematically in the adjacent isobaric plot are located on the phase lines (dashed) numbered with the same boxed numerals as shown in Fig. 4. Frequency-temperature dependencies show obvious slope sign changes at ~ 120 and 195 GPa, respectively.

additional supporting evidence. Solid lines in the figure are the polynomial fit used to yield smoothed sections separated by the frequency discontinuities, which offer a way for sorting isobaric temperature dependencies of vibron frequency at desired pressures. When data points suggest a series of rapid slope changes from negative to positive and to negative again, as shown to occur above 235 or 229 GPa in Fig. 2 (left), smoothed curves have been selected as the default interpretation. We believe that its influence on the evidence for phase transitions has only a slight effect on the interpretation. A total of 27 isotherms with incremental temperatures are obtained and are listed in Fig. S4 of the SM [18].

The second step is to establish isobaric frequency-temperature (FT) relations based on the fitted isothermal frequency-pressure (FP) dependencies as described above. Figure 3 left presents the respective plots for the temperature trend of the ν_1 frequency obtained during two constant-force-loaded heating runs and the isobaric corrections using the isothermal fitting results. The measured peak-width (FWHM) variations for vibron ν_1 are also shown as insets. Some isobaric plots clearly reveal significant FT discontinuities which were not observed during the constant-force-loaded heating runs. This is because the accompanying pressure change modified the whole heating frequency trajectory demonstrating the situation we have discussed above. Similar to the isothermal plot, the consistency between discontinuities of frequency and

peak width is observed for many transitions. Figure S5 of the SM [18] lists 27 similar isobaric plots at different pressures.

III. OBSERVATIONS AND DISCUSSIONS

The room-temperature findings of vibron frequency first decreasing with pressure above ~ 30 GPa, and having a significant slope decrease at around ~ 216 – 220 GPa, have been well established experimentally [9,12,14]. At higher temperatures, we found that the starting pressures for the steeper slope vary with temperature and that the isothermal curves show much more complicated details, suggesting that they are crossing over multiple different phase boundaries (Fig. 2, left and Fig. S4 of the SM [18]). Since the data points come from different independent constant-force-loaded heating runs, they unavoidably suffer small random scattering (standard deviation $\sigma = \sim 4$ – ~ 10 cm^{-1}). However, a statistically smoothed sectional tendency between obviously larger discontinuous points ($\Delta = \sim 20$ – 45 cm^{-1}) provides evidence for the phase changes. This is especially true; if frequency discontinuities appear in a series of adjacent isothermal plots as shown in Fig. 2 (right), those discontinuities have a high probability of representing a series of solid-solid phase transitions along a phase boundary. Because each discontinuity is formed not by one but by multiple measured PT points, each of which comes from an independent heating run of a freshly loaded sample,

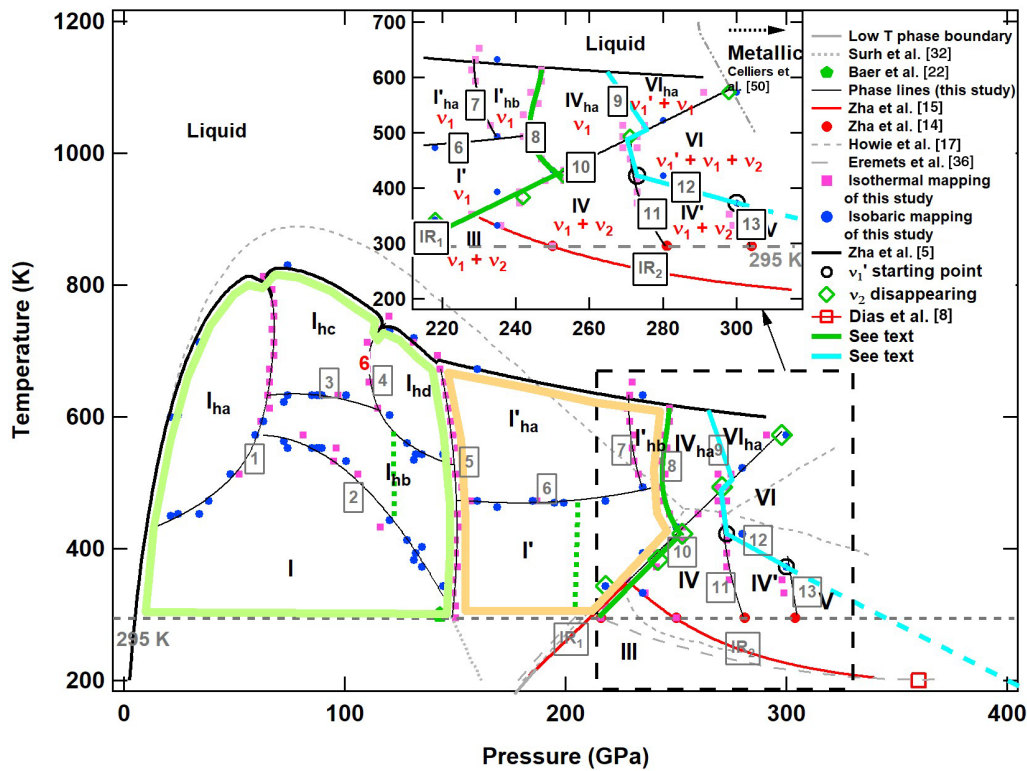


FIG. 4. Potential phase diagram of hydrogen. Pink squares and blue solid dots are the phase transition points from isothermal and isobaric network mapping. Black thin solid lines are phase boundaries found in this study and numbered with gray boxed numerals. Bold Roman numbers with or without subscripts are the names of hydrogen phases. Other symbols and lines are indicated in the figure legend. Two green dotted lines indicate the position of frequency-temperature slope change ($dv/dt = 0$) within phases I_{hb} and I' , respectively (see text). Phase areas enclosed by thick, light green, and light yellow polygons are the two isostructure phase regions described in the text. Inset is an enlarged area showing details of multiple vibron modes appearing/disappearing in the dashed rectangular portion of the main drawing. The broad green and light blue lines are the starting boundaries for the strong anharmonic structure and a new vibron v'_1 appearing, respectively (see text).

they thus offer a statistically reliable way for distinguishing randomly introduced kinks and other discontinuities by any source other than the sample.

Isotherms presented in this way also have the advantage of reducing or eliminating all possible systematic pressure-frequency errors that could occur during single isothermal compression runs. In addition, averaging by statistical probability (curve smoothing) may help to reveal a few very small discontinuities such as those found at a point, for example, at ~ 150 GPa and 295 K, which has not been reported in most previous room-temperature compression experiments except for one. [22] Actually, this point also provides evidence for a triple point as there is a new phase I_{hb} appearing between phase I and phase I' as we will show in Fig. 4. It is not surprising that the majority of FP discontinuities, if not all, appear simultaneously with those of peak width at the same PT conditions as shown in the plots (Figs. 2 and S4 of the SM [18]); this self-consistency provides evidence for the reliability of the measurements.

Temperature dependencies of vibron frequency also reveal some variations that are rarely seen in pressure dependence. For example, we observed that the negative slope of the FP (dv/dp) almost dominates the changing tendency in most pressure ranges (Fig. S4 of the SM [18]) except one phase area, where a unique behavior for phase I_{hb} (Fig. 4) is observed. It shows a positive slope of dv/dp for vibron v_1

(see Fig. S4 of the SM, 11–18). In contrast, the slope of FT dependence (dv/dt) shows complicated fluctuations at different PT ranges. For example, if we systematically check the temperature dependence of vibron frequency in Figs. 3 and S5 [18] (14–17), the dv/dt corresponding to the new phase I_{hb} area changes from a positive value at lower pressure to a negative one at higher pressures. The turning point ($dv/dt = 0$) appears at pressures around ~ 120 – ~ 128 GPa (see Fig. S5, 15 and 16, of the SM [18]). Similarly, the slope value of the dv/dt changes from negative to positive; this happens at ~ 195 GPa (see Fig. 3, right, or Fig. S5 of the SM [18] before and after 24). However, no sharp discontinuity was found in the isothermal FP plots (see Fig. S4 of the SM [18]) crossing these two turning areas, indicative of the possible existence of higher-order transition boundaries as shown by two green dotted lines in Fig. 4.

A total of 54 isothermal and isobaric plots were obtained and carefully analyzed as presented in the Supplemental Material (Figs. S4 and S5) [18]. All the P - T points showing discontinuous frequency, peak width, and slope changes found in either of these two types of plots were chosen to define the possible phase boundaries. Figure 4 represents the plot of all those transition PT points. Their locations clearly suggest phase boundaries and represent a potential phase diagram of the solid phases of hydrogen. Points derived from individual isothermal plots are mostly located on those boundaries

having approximately vertical orientations, and the points derived from isobaric plots are mostly located along the horizontal boundaries. Curved and diagonal boundaries are constructed by the mixed data points found from both the isothermal and isobaric plots. This is critical evidence showing that the results from two sets of thermodynamic mapping are self-consistent.

We found in the lower pressure-temperature range that the shapes of the FP dependence for vibron ν_1 , at all temperatures, display a great similarity in two regions, respectively, as shown in the selected isothermal plots of Fig. S6 in the SM [18]. We highlighted these two pressure regions with broad lines in light green and yellow, respectively, in Fig. 4. In these two pressure regions, only one vibron was observed. The phase transitions were characterized mainly by discrete shifting in both vibron frequency and peak width. Although the observed discontinuities of vibron frequency between the respective phases in these two regions are quite obvious, the changing magnitudes are generally not very large ($\Delta\nu = \sim 20\text{--}45\text{ cm}^{-1}$ compared to random data scattering of $\sigma_\nu = \sim 4\text{--}10\text{ cm}^{-1}$). The increases of peak width as functions of pressure and temperature do not show a noticeable discontinuity in the most defined phase lines except for phase line 5 which is the boundary between these two areas. An example of the not very large frequency difference for the vibron from the two sides of this phase line is shown in Fig. S7 of the SM [18]. We postulate that these features of vibron ν_1 are an indication of structure similarities in these two phase areas, most likely suggesting that the transitions are some kind of isostructural transition [23]. Therefore, the new phases found in these two regions are labeled on the basis of their low-temperature identification label with subscripts “h” and sequential alphabetical letters meaning high-temperature phases. Four new phases at locations above phase I in the first phase region are named I_{ha} , I_{hb} , I_{hc} , I_{hd} , whereas two new phases at positions above phase I' in the second region are named I'_{ha} , and I'_{hb} . This typical assignment helps remove ambiguity and confusion with previous studies.

IV. LOW-FREQUENCY SPECTRA EVIDENCE

Principally, structure transition indicated by abnormal change in the high-frequency intramolecular vibrational Raman mode (vibron) should have a corresponding change in the low-frequency rotational and lattice modes. Unlike the single, strong mode of vibron, obtaining high-quality, explicit low-frequency spectra has been a technical challenge at high pressure above the room temperature because of its weakness and pressure-temperature broadening nature for the multiple modes. Because we benefit from technical improvements, we are able to collect many good low-frequency spectra from 2 GPa all the way to 300 GPa at and above 300 K. Figures 5 and S8 in the SM [18] show the representative spectra and its pressure-temperature dependence, respectively. At very low pressures, our data show four rotational bands that agree with frequencies of $S_0(0) = 6B$, $S_0(1) = 10B$, $S_0(2) = 14B$, and $S_0(3) = 18B$, approximately, if assuming a free rotation model exists, where B is the rotational constant with $B(\text{H}_2) = 59.3\text{ cm}^{-1}$ at gas phase [24]. It is fortunate

that the strongest rotational mode $S_0(1)$ (before it splits at 216 GPa) and clear lattice phonon peak E_{2g} [when crossed over the mixing range with the $S_0(1)$ mode] can be well located at the whole pressure-temperature range for tracing their change. The pressure dependence of two former rotational bands and lattice phonon E_{2g} we obtained at room temperature is generally consistent with previous measurements at lower [25] and higher [12,14,26] pressure ranges, respectively, while peak evolution of L_4 is found to be different from some previous reports [12,26] as shown in the upper part of Fig. 5.

Our data show interesting features appearing above ~ 150 GPa where frequencies of rotational bands $S_0(0)$ and $S_0(1)$ are gradually coming close together with increasing pressure [see the upper part and panel (d) of the lower part in Fig. 5]. It means the rotation constant B , which is based on the free rotation assumption, becomes inconsistent for each rotation band and the free rotation assumption is no longer the proper description. This mixing situation persists to ~ 216 GPa and then is split into three bands called L_1 , L_2 , L_4 , while the E_{2g} band continues to 250 GPa; then it changes slope and is called L_3 [26] [also see panel (e) of Fig. 5, lower part].

Previous experiments conducted at room temperature, and this study, mostly use vibron discontinuity as the indication of phase transition. Four discontinuities at room temperature were claimed at ~ 150 [22], 216–220 [9,12,14,15], 250 [14,15], and 270–280 [9,14,28] GPa. The later three transitions are reported accompanied by a significant change in low-frequency Raman modes; however, the transition at 150 GPa showed a lack of explicit low-frequency supporting information. One of the reports, involving the low-frequency behavior of hydrogen in the pressure range of $\sim 150\text{--}216$ GPa [14], did show abnormal $S_0(0)$ and $S_0(1)$ changes similar to those described above (see Fig. 5 of Ref. [14]) but with no confident discussions. The obvious reasons were as follows: on one hand, no vibron frequency discontinuity was found at ~ 150 GPa from the room-temperature isothermal compressions of that study; on the other hand, the relatively weak and broadened low-frequency spectra at this pressure range were only collected from limited experimental runs. This needs to be confirmed by more experiments. Now, the complete set of low-frequency Raman spectra, collected from the room-temperature starting pressure points of more, different heating runs, also shows consistent results. Considering the vibron discontinuity analysis above, which revealed a triple point merged by phase lines 2 and 5 at 150 GPa as shown in Fig. 4, the abnormal change in low-frequency Raman at the same point adds much confidence for both previous and present findings. The significant frequency change for $S_0(0)$ and $S_0(1)$ at the breadth of 150–216 GPa demonstrates that the gradual monotonic rotational change below 150 GPa begins a dramatic, large-scale rotational (librational) change at this point and continues to 216 GPa, at which a new (possibly layered) structure (phase III) is created [3,29,30]. The breadth between these two points is named phase I' [22,31,32] for consistency with previous research. In addition, lattice phonon peak E_{2g} shows up at all temperatures also confirming that the transitions crossing over phase line 5 are not a significant symmetry change. Hexagonal close packed lattice provides the stable symmetry at both sides of phase line 5 [33,34].

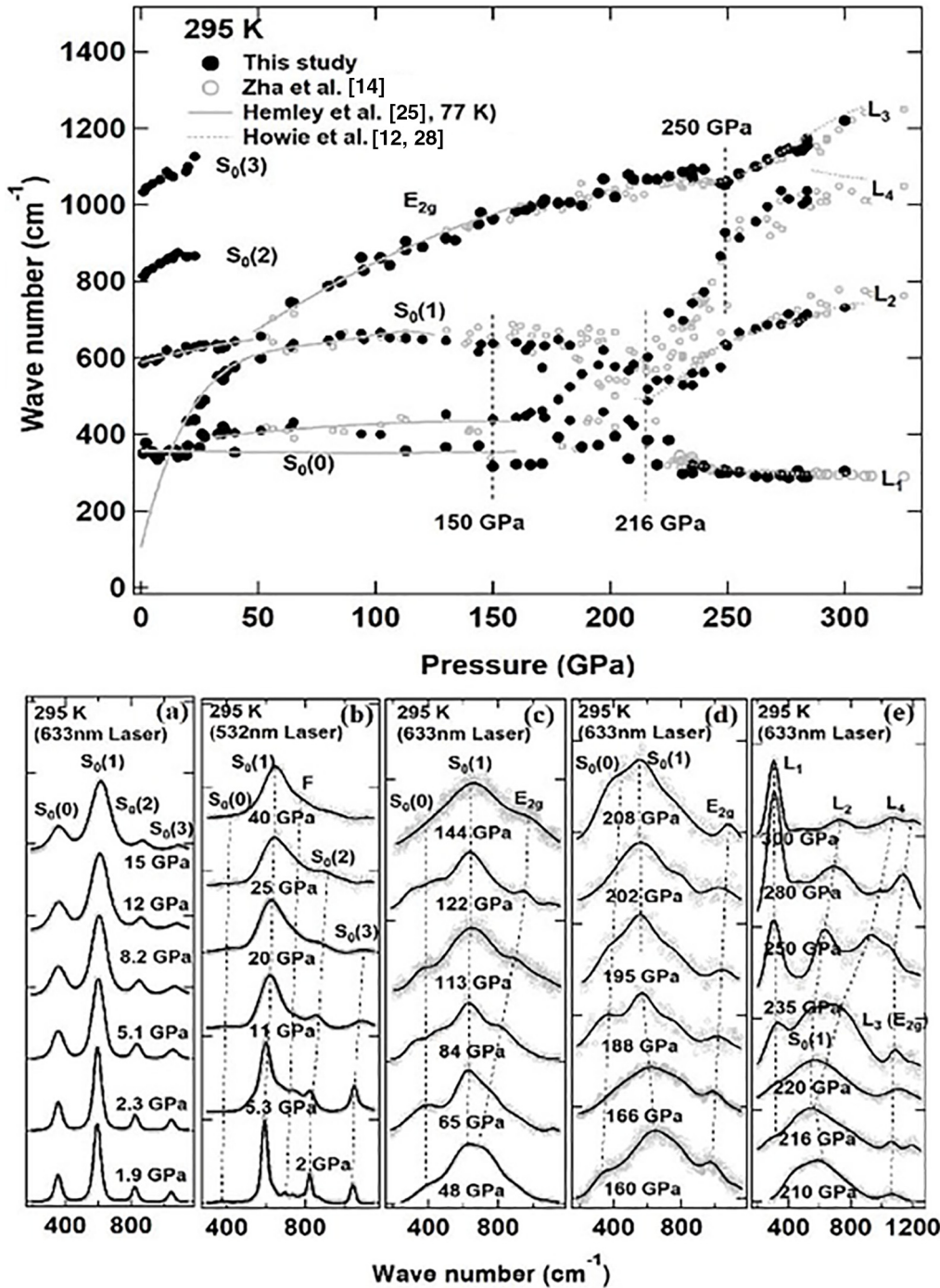


FIG. 5. Low-frequency Raman data at room temperature are obtained from multiple isothermal, as well as the starting pressure points of different heating experimental runs. Upper panel: FP dependencies of four rotational and lattice phonon bands, respectively. Lower panel: representative Raman spectra for rotational bands $S_0(0)$, $S_0(1)$, $S_0(2)$, $S_0(3)$, and lattice phonon band E_{2g} at different pressures. Different from low-temperature spectra [25,27], the $S_0(1)$ band is the strongest peak among the all bands at (and above) room temperature no matter whether different laser excitation wavelengths are employed; it can be easily located until 216 GPa (e). Diamond fluorescence [F in (b) of lower panel] may appear when higher excitation energy is used. All rotational bands are broadened with pressure significantly, $S_0(2)$ and $S_0(3)$ are diminished fast with pressure, and become irresolvable at pressure higher than ~ 25 GPa [see (b) of lower panel] (b). At room temperature, lattice phonon E_{2g} (L_3) can be seen until the highest pressure of this study.

Low-frequency spectra also provide evidence supporting the new phases derived by minor vibron changes found at high temperatures in the two phase areas enclosed by broad color lines in Fig. 4. Frequencies of the rotational bands are

found to be insensitive to temperature and there is only a weak pressure shift in the low-temperature experiments [25,27]. However, we do find obvious frequency-temperature kinks for the E_{2g} phonon and $S_0(1)$ band. Kinks always appear when

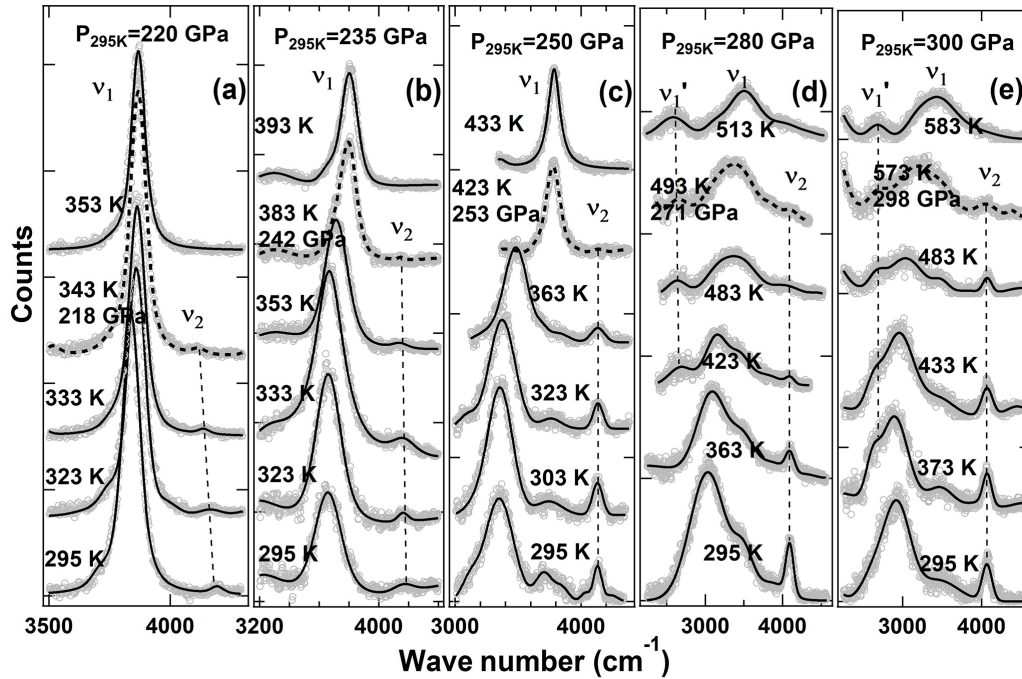


FIG. 6. Vibron ν_2 spectra change with temperature during the constant-force-loading heating at different starting pressures. The dotted spectrum at each panel shows the last appearance of vibron ν_2 at this heating run. A new peak ν'_1 appears at the two highest-pressure heating runs as shown in (d), (e). Unmarked peaks (or shoulders) to the right of ν_1 are the fluorescence peak (see Fig. S9 of the SM [18]); its intensity seems diminished with increasing temperature.

heating trajectories cross over the phase boundaries as shown in Fig. S8 of the SM [18]. This demonstrates that the subtle high-temperature phases found by minor vibron discontinuities also are accompanied by a corresponding change in the low-frequency Raman modes. The rotational state may significantly affect the solid hydrogen's structure and electronic properties at high pressures, but little information for the temperature effect was known. Temperature-induced changes in low-frequency Raman spectra offer even richer structural information which may help future theoretical study for better understanding the complex mechanisms of structure change in hydrogen.

V. TRANSITIONS AT PRESSURE HIGHER THAN ~ 216 GPa

The more interesting and possibly important phase transitions of this study were found when the pressure-temperature values reach over phase lines 10 and 8. The transition at approximately $216\text{--}220 \pm 15$ GPa and 300 K was reported previously [9,12,14,26], featuring a sudden change in the dv/dp slope of ν_1 and peak width broadening. Also, a weak second vibron ν_2 (Fig. 6) as well as a lattice mode L_1 have started to appear [see the lower portion of Fig. 5, panel (e)]. Theoretical simulations indicate that the phonon frequencies of a new layered structure are consistent with the experimental observations (phase IV). [4,29,40–42] This transition is consistent with our finding in the present study at 216 GPa and 295 K on phase line 10 of Fig. 4. However, disputes concerning the ν_1 vibron behavior after this point, which defines the phase boundary between phases III and IV (see Fig. 4), exist. First, the reported pressure range for phase III along the isotherm of 300 K was inconsistent among different studies

[14,15,28,35]. Second, the sudden dv/dp slope downward trend and the peak width broadening of ν_1 are separated from the appearance of the second vibron peak ν_2 in some previous reports. This is inconsistent with theoretical predictions. [4,42] Our finding suggests this pressure range should be between 216 and 250 GPa, and the second Raman vibron peak of ν_2 as well as the lattice mode L_1 , appears simultaneously with the down-slope of ν_1 frequency and peak width broadening at 216 GPa and 295 K though the intensities of the ν_2 are very weak in the phase III range. [14] It is important to note that the reported room-temperature slope of dv/dp for vibron ν_1 after entering phase III is consistent between different groups (see Fig. S3 of the SM [18]), but very different from that observed at the low temperature of phase III. [12,14,36,37] Combined with the appearance of weak peaks of ν_2 and L_1 at and above 300 K, the structure of solid hydrogen in the upper region of phase III might not be simple. Possibly some modified structures exist at that portion, and more detailed PT mapping work needs to be conducted in the phase III region.

A weak second vibron peak ν_2 at $\sim 4200\text{ cm}^{-1}$ found experimentally [9,12,14,26,36] at $\sim 216\text{--}\sim 235$ GPa and 300 K has stimulated intense theoretical work in recent years. It has been widely attributed to a layered structural change. [4,29,38–42] Causatively, the disappearance of this high-frequency vibron of ν_2 would be the indication of a phase change (or decomposition) for the layered structure. In this study, the layered structure was found to be unstable at high temperatures as indicated by the disappearance of vibron ν_2 during heating. Figure 6 shows the spectra of solid hydrogen in five heating processes started at different pressures. The ν_2 vibrons in all five runs weakened upon increasing temperature and disappeared at various temperatures in different runs. The

PT points for the last appearance of the ν_2 peak during heating are plotted in Fig. 4 (green open diamond symbol); they nicely coincide with phase line 10 and infrared-determined IR_1 . [15] It seems that the line can be extended smoothly to align with the I'–III transition line at low temperature. Phase line 10 represents a significant boundary that divides the phase space of solid hydrogen into two portions, distinguished by the presence and absence of a second vibron on each side. A more detailed picture is that the appearance of a significant downward turn for the dv/dp slope and the ν_2 peak disappearance happens simultaneously at the initial stage and proceeds together for a while. The temperature values for this situation increase with pressure along the phase line 10 from ~ 216 GPa at 295 K to ~ 253 GPa and 433 K, which is the intersection of phase lines 10 and 8. At this point, pressure for the downward turn of the dv/dp slope stops increasing, and the downward slope appears along phase line 8 while the vibron peak ν_2 disappearance is still tracking with phase line 10 to the highest pressure of this study (see Fig. S4 of the SM [18]). Discontinuous frequency points of vibron ν_1 detected throughout isothermal and isobaric plots are also located along phase line 10 (Fig. 4). This indicates that the phase transitions crossing over this phase boundary show both mode appearance and disappearance and frequency discrete shifting. The consistency between the two types of measurements confirms the reliability of line 10 as a phase transition boundary. The collection of all the information allows us to conclude that phase lines 10 and IR_2 represent the higher and lower temperature boundaries of phase IV, respectively (Fig. 4).

We wish to point out the existence of an important phenomenon for vibron ν_1 revealed in this study. It is apparent that the significant downward slopes of dv/dp always come with peak widths that suddenly broaden at all PT conditions (as shown in Fig. S4 and its insets, in the SM [18]). This is an indication of a strong change in structure anharmonicity. The PT trend along with phase lines 10 and 8 discussed above is shown as a broader green solid line in Fig. 4. High-pressure phases to the right side of this green solid line are all involved. This finding extends the previous room-temperature observation [9,12,14,26,43] to a very large PT zone and could inspire future theoretical studies on structural investigation of the hydrogen system.

The layer-structured hydrogen shows even more complicated phase transitions at the higher pressure-temperature regions. Previous room-temperature studies found a very slight pressure slope change of band gap and Raman vibron ν_1 . [28] Also, an abrupt intensity change for the lowest libron L_1 around 275–285 GPa was reported. [14] These have been attributed to a structural transition to phase IV'. The reported observation for loss of the Raman mode and the sample turning to a dark, electrically conducting state at similar pressure was not reproduced. [9] The phase line 11 found in this study reveals that dv/dp slope changes for vibron ν_1 around this pressure range are indeed too weak to find at temperatures below 353 K (see Figs. 4 and S4 of the SM [18]). Instead, the intensity change of the lowest lattice mode L_1 in this pressure region is very obvious even below 353 K as shown in Fig. 7 [compare panels (c,d)]. However, the dv/dp slope change for vibron ν_1 becomes very obvious starting from 353 K up to 513 K (Fig. S4 of the SM [18]). This feature characterizes the

higher-temperature portion of phase line 11. Obviously, phase line 11 is the boundary between phases IV and IV'. The PT point of 271 GPa and 493 K is the intersection point of phase lines 11 and 10 (Fig. 4). At temperatures above this point, ν_2 disappears [see Fig. 6(d)], indicative of the existence of a new phase. The slope of FP dependence for ν_1 in this region drops down steeply, similar to that in phase IV (see pressure range higher than phase line 8 in Fig. S6 of the SM [18]), but very different from phase I'_{hb} (which is the only region with a positive slope for FP dependence), so it is named phase IV_{ha}.

Room-temperature studies have also reported another possible transition to phase V around ~ 300 – 325 GPa at 295 K [14,26,35] or vicinity temperature range. [35] Here, we found that phase IV' seems to be terminated at phase line 13 as defined by the slight frequency discontinuity of ν_1 in isothermal plots at 333 and 353 K. It is a little lower than 300 GPa (Fig. S4 of the SM [18]), consistent with the previous report. This short line ends when temperature increases to 373 K, at which point a new peak ν'_1 starts to appear [see Fig. 6(e)]. This indicates that another new phase transition happens at a higher-temperature region. Pressure higher than phase line 13 should be the phase V area (see Fig. 4). No additional data are available to define the phase boundaries in the higher-PT range for phase V.

As already mentioned above, an interesting thing to note is that a new peak ν'_1 is found in two higher-pressure heating runs. During the first heating run with starting pressure of 280 GPa, the peak appears when the temperature reaches 423 K and the *in situ* pressure at 273 GPa. The peak is on the lower-frequency side of vibron ν_1 [Fig. 6(d)] at ~ 2690 cm^{-1} . The same peak appears also in the heating run at a starting pressure of 300 GPa, but at a lower temperature of 373 K [see Fig. 6(e)] and *in situ* pressure of 299 GPa with a similar frequency. These have been attributed to the vibron mode of new phase *Cmca-4* reported previously. [5] Because of this new peak, a new phase boundary can be drawn from these two PT points as phase line 12, together with phase lines 10 and 11, forms a new phase VI as illustrated in Fig. 4. This phase is featured with three Raman vibron modes of ν_1 , ν_2 , and ν'_1 [inset of Fig. 4, and Figs. 6(d) and 6(e)]. Figure 8 shows the temperature-frequency trajectory during these two heating runs. Frequency of the ν'_1 shows an approximate stable pressure dependence when it appears, but a slightly different temperature dependence during these two heating runs.

Upon further heating from phase VI to cross over phase line 10, phase VI transforms to another new phase because it lost vibron ν_2 , with only two vibrons ν_1 and ν'_1 remaining (inset of Fig. 4). The heating path started at 280 GPa is along phase line 9 and thus enters the region of phase IV_{ha} (Fig. 4). As mentioned above, phase IV_{ha} has a vibron peak ν_1 only, but there are currently two vibron peaks. Obviously, phase line 9 is a new phase boundary as indicated by the appearance of the new peak. The name for this new phase is VI_{ha}. It is unusual that phase line 9 does not show a frequency discontinuity for vibron ν_1 when checking the frequency-pressure dependence between these two phases from the isothermal plots (see 13–17 in Fig. S4 of the SM [18]). Pressure-induced phase transition involving the appearance of new peaks usually is accompanied by a discrete shift of the peak frequencies. The continuous ν_1 frequency from phase IV_{ha} to VI_{ha} implies that

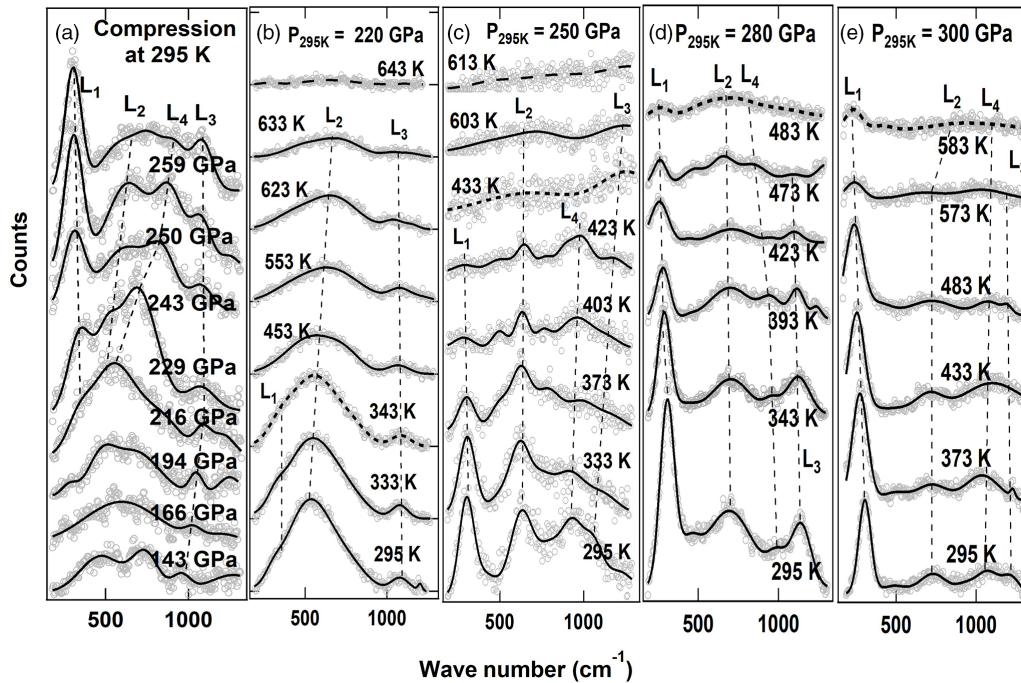


FIG. 7. The behavior of librons at high pressures and temperatures. Panel (a) shows the libron spectra under isothermal compression at 295 K. The broad libron peak at lower pressure is split into L_1 , L_2 , and L_4 after 216–220 GPa which is the I' to III phase transition point at room temperature. Panels (b)–(e) show how the librons change with increasing temperature at selected heating runs. Dotted line spectra are collected at the PT points corresponding to ν_2 vibron disappearance (see Fig. 6). Dashed-line spectra in (b), (c) are collected at the melting point. In the heating runs with starting pressure ≤ 250 GPa in (b), (c), L_1 and L_4 [the L_4 can be seen only in panel (c) because it has not separated enough from L_2 at 220 GPa] disappear simultaneously along with the disappearance of the ν_2 vibron, while L_3 does not and persists to the melting line; these happen within phases I' , I'_{hb} , and IV_{ha} . However, heating runs with starting pressures of 280 and 300 GPa in panels (d), (e), both libron L_1 and L_4 no longer disappear simultaneously with ν_2 ; instead, only L_3 does. These happen within phase VI_{ha} .

new peak ν'_1 does not have a structural relationship with vibron ν_1 in phase VI_{ha} . Therefore phase VI_{ha} may not be a new single phase with two vibrons. Phase VI_{ha} most likely is multiple phases, where ν_1 and ν'_1 belong to different phase components. On the other hand, the continuous ν_1 does not necessarily mean the structure, which ν_1 belongs to at phase area VI_{ha} , is the same as that of phase IV_{ha} . It might only be just a numerical coincidence for the frequency. This assertion is supported by the lattice mode behavior at high temperatures as shown in Fig. 7. The evidence presented in Figs. 7(d) and 7(e) clearly shows the lattice mode behaviors of phase VI_{ha} are different from that of phase IV_{ha} [Fig. 7(c)]. Librons L_1 and L_4 along with ν_2 vibron disappeared at 433 K, but not for L_3 in phase IV_{ha} . However, heating runs in Figs. 7(d) and 7(e) show that both libron L_1 and L_4 no longer disappeared with ν_2 at 483 or 583 K. Only L_3 disappeared along with it; this happened in phase VI_{ha} . The disappearance of lattice mode L_3 within phase VI_{ha} indicates that the phase component contributing the ν_1 vibron likely no longer belongs to the hcp structure system according to the analysis of previous studies [25,33,34] and is apparently different from phase IV_{ha} .

VI. POSSIBLE MOLECULAR DISSOCIATION TO METALLIZATION

More structural information represented by the behavior of peak ν_1 , ν_2 , and ν'_1 during heating may be extracted from Fig. 8. First, the appearance of ν'_1 and disappearance of ν_2

is always accompanied by a discontinuous frequency change in ν_1 . This means that ν_1 is connected with both ν_2 and ν'_1 . Second, when ν'_1 appears, or ν_2 disappears, nothing happens on the other one, indicating no connection between these two modes, i.e., new peak ν'_1 is only related to the graphenelike layer of phase IV' (assuming the structure of phase IV' is very similar to phase IV as previously proposed [28]). The above observations suggest the ν'_1 might originate from a progressive dissociation of graphenelike layers at the higher temperature. The dissociation would result in a frequency discontinuity of ν_1 whereas the disappearance of ν_2 might result in the second large shift in ν_1 but not in ν'_1 . After dissociation, ν_1 and ν_2 are still from two layers of a phase component, which is the phase nonrelated to ν'_1 . The component from dissociation featured with peak ν'_1 is a separate entity that coexists before and after the disappearance of ν_2 , indicating that both VI and VI_{ha} exist in multiple phase areas (see inset of Fig. 4). We note that, although the frequency uncertainty due to pressure change during heating in Fig. 8 was not corrected, we think the total change of ~ 10 GPa for the entire heating run, without an obvious sudden jump up or down being recorded, does not affect the main frequency feature discussed here.

Crystal structure prediction based on density-functional theory (DFT) and *ab initio* random structure searching algorithms have been mostly used for predicting possible structure candidates of solid hydrogen at high pressures. [3,4,29,39,44–48] Phonon frequency spectra of candidate structures

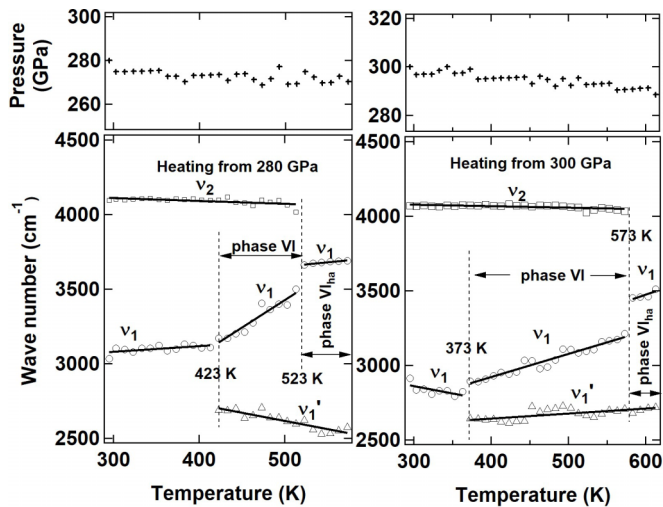


FIG. 8. Temperature dependence for three vibration modes at two heating runs reveal interesting structure relations between the possible phase transitions during the heating. Symbols: measured data; solid lines are for guiding the eye. Double arrows show temperature range for phases VI and VI_{ha} during two heating runs. Frequency modulations by pressure variation during heating were not made because no reliable isothermal fitting data are available at this high-pressure range.

calculated over a wide pressure range for comparison with experimental results were the direct way for checking the reliability of the theory. Among many candidate structures, phonon frequencies for $Cmca-4$, [5,47] $I4_1/amd$, and $R-3m$ structures [44] are reported to be close to that of vibron ν'_1 found in our experiments though the predicted stable pressure ranges are different. A common characteristic of these candidate structures is that they are all metallic. This means that a predicted metallic state indeed appears at the particular region of the hydrogen phase diagram. This transition process may not simply have a sharp, single boundary; it could be a multiple transition process involving a period where a metallic-nonmetallic mixture exists. We also find that the phonon frequency ν'_1 , if it can serve as a possible sign of metallic transition according to theoretical predictions, prefers to appear at higher temperatures while pressure could be lower or vice versa, consistent with the big picture built by most previous reported experiments [35,49–53] and theoretical predictions. [3,4,45,54–57]

On the other hand, the disappearance of ν_2 at higher temperatures indicates that the structure for the disordered molecular layer of the phases (presumably including phases III, IV, and VI) is unstable upon heating; it dissociates at temperatures above phase line 10, and re-forms into the new phases of I' , IV_{ha} , and VI_{ha} . The transition is also accompanied by the ν_1 frequency discrete shift from phases III, IV, and VI. As discussed above, since both the phase VI and VI_{ha} regions are probably the coexisting multiple phases, we can draw light-blue lines in Fig. 4 as the boundary of multiple phase regions in which ν'_1 exists. The region is enclosed by phase lines 9–12 in the solid phase area with an open side to the liquid area. Although not enough data are used to ascertain the behavior of ν'_1 , we cannot rule out the possibility for the

existence of peak ν'_1 in the liquid area as seen in Figs. 2(d) and 2(h) of Ref. [5].

Figure 8 shows that the ν_1 frequency decreases significantly with increasing pressure, but ν'_1 is relatively stable when it appears. The frequency difference between ν_1 and ν'_1 therefore decreases with increasing pressure, and the two peaks are expected to overlap at higher pressures. If ν'_1 owes its origin to the progressive dissociation of the graphenelike layer of phase IV' as suggested above, the overlapping should indeed be a replacement. This means that the ν_1 peak should finally be replaced by ν'_1 , presumably happening somewhere as extrapolated by the light-blue dashed line in Fig. 4. Further experiments at higher pressure are required to confirm this prediction.

VII. SUMMARY

In this study, we present a large amount of physical evidence for the phase transitions of dense solid hydrogen in a broad pressure-temperature range, which occupies important phase space. The data analyzed here are collected during many independent constant-force-loaded heating runs, and each of them includes numerous stepwise temperature increments and different starting pressures. With the advantage of reducing systematic uncertainties by network analysis, which is obtainable only by collecting a large amount of data at incremental P and T points, the results demonstrate that not only most previously identified transitions reported at room-temperature compression experiments are nicely verified, but also a surprisingly rich and complex assemblage of collected phase transitions at a higher-temperature range are revealed. Interestingly, they also show the sensitivity capable of finding some minor changes in the lower-pressure but higher-temperature range. We confidently present these minor changes as the true transitions instead of the experimental errors, because we believe random errors do not produce the discontinuities which were sequentially, regularly connected by phase lines (see Figs. 2 and S6 of the SM [18]); they especially show good self-consistency as discussed in the text. It may seem odd that the simplest element should have such a complex phase diagram. However, it also seems odd that such a simple material should have a spectrum with an extensive range of absorption and emission lines when it was found more than a century ago. The answer for the latter has been known by modern quantum theory and used by scientists in many disciplines. Unfortunately, how simultaneous high pressure and high temperature affect the phase conditions of solid hydrogen still is poorly understood. There has been a dearth of research in this respect both experimentally and theoretically. It is noteworthy that a recent calculation [58] proposes the possibility that significant changes in the Raman spectrum may be insufficient to demonstrate a phase transition. Those situations remind us that the phase boundaries based on the mapping of Raman spectroscopy could be provisional. We expect that the primary results obtained in this study certainly will inspire more experimental verification studies for both validities of phase transitions and the precision of boundary positions. On the other hand, the complicated Raman change may be proven not to relate to the phase transition as proposed by the above calculation. The unknown significance behind

the Raman change should also stimulate more theoretical investigations for a better understanding of its properties in this virgin phase territory.

The most interesting findings in this study are those located in the PT range greater than ~ 216 GPa and high temperature up to the melting line. Our phase mapping has revealed spectroscopic evidence that phonon frequency consistent with most predicted metallic states indeed appears at the particular PT conditions. Also, the appearance and disappearance of the multiple Raman peaks as well as the coincidence with a discrete frequency shift of ν_1 vibrons offers rich information for understanding the possible phase evolution. Molecular hydrogen likely undergoes a gradual dissociation process before its metallization transition. Explanations of such a phase evolution will be of great theoretical interest in the future. It

certainly will revise our current theoretical understanding of this simplest element.

ACKNOWLEDGMENTS

The authors are grateful to Z. Gebarlle, T. Strobel, John Tse, R. J. Hemley, T. S. Duffy, and Y. M. Ma for useful discussions. The original data reanalyzed in this work were collected under the support of CDAC (Carnegie/Department of Energy Alliance Center, Grant No. DE-NA-0002006) and EFree (Energy Frontier Research Center, Grant No. DE SC0001057) research programs. C.-S.Z. is grateful for the Carnegie community's invaluable support. The CHESS is partially supported by the NSF Awards No. DMR-1332208 and No. DMR-1829070.

-
- [1] I. Silvera, The bizarre properties of solid hydrogen at high pressure, in *Proceedings of the Joint 20th AIRAPT and 43rd EHPRG International Conference on High Pressure Science and Technology*, edited by E. Dinjus (Forschungszentrum Karlsruhe GmbH, Germany, 2005).
- [2] E. Wigner and H. B. Huntington, On the possibility of a metallic modification of hydrogen, *J. Chem. Phys.* **3**, 764 (1935).
- [3] C. J. Pickard and R. J. Needs, Structure of phase III of solid hydrogen, *Nat. Phys.* **3**, 473 (2007).
- [4] J. McMinis, R. C. Clay, III, D. Lee, and M. A. Morales, Molecular to Atomic Phase Transition in Hydrogen under High Pressure, *Phys. Rev. Lett.* **114**, 105305 (2015).
- [5] C. S. Zha, H. Y. Liu, J. Tse, and R. J. Hemley, Melting and High P - T Transitions of Hydrogen up to 300 GPa, *Phys. Rev. Lett.* **119**, 075302 (2017).
- [6] H. K. Mao and R. J. Hemley, Ultrahigh-pressure transitions in solid hydrogen, *Rev. Mod. Phys.* **66**, 671 (1994).
- [7] A. F. Goncharov, R. T. Howie, and E. Gregoryanz, Hydrogen at extreme pressures (Review Article), *Low Temp. Phys.* **39**, 402 (2013).
- [8] R. P. Dias, O. Noked, and I. Silvera, Quantum phase transition in solid hydrogen at high pressure, *Phys. Rev. B* **100**, 184112 (2019).
- [9] M. I. Eremets and I. A. Troyan, Conductive dense hydrogen, *Nat. Mater.* **10**, 927 (2011).
- [10] M. I. Eremets, I. A. Troyan, P. Lerch, and A. Drozdov, Infrared study of hydrogen up to 310 GPa at room temperature, *High Pressure Res.* **33**, 377 (2013).
- [11] E. Gregoryanz, A. F. Goncharov, K. Matsuishi, H. K. Mao, and R. J. Hemley, Raman Spectroscopy of Hot Dense Hydrogen, *Phys. Rev. Lett.* **90**, 175701 (2003).
- [12] R. T. Howie, C. L. Guillaume, T. Scheler, A. F. Goncharov, and E. Gregoryanz, Mixed Molecular and Atomic Phase of Dense Hydrogen, *Phys. Rev. Lett.* **108**, 125501 (2012).
- [13] P. Loubeyre, F. Occelli, and P. Dumas, Hydrogen phase IV revisited via synchrotron infrared measurements in H_2 and D_2 up to 290 GPa at 296 K, *Phys. Rev. B* **87**, 134101 (2013).
- [14] C. S. Zha, R. E. Cohen, H. K. Mao, and R. J. Hemley, Raman measurements of phase transitions in dense solid hydrogen and deuterium to 325 GPa, *Proc. Natl. Acad. Sci. USA* **111**, 4792 (2014).
- [15] C.-S. Zha, Z. Liu, M. Ahart, R. Boehler, and R. J. Hemley, High-Pressure Measurements of Hydrogen Phase IV Using Synchrotron Infrared Spectroscopy, *Phys. Rev. Lett.* **110**, 217402 (2013).
- [16] C.-S. Zha, Z. Liu, and R. J. Hemley, Synchrotron Infrared Measurements of Dense Hydrogen to 360 GPa, *Phys. Rev. Lett.* **108**, 146402 (2012).
- [17] R. T. Howie, P. Dalladay-Simpson, and E. Gregoryanz, Raman spectroscopy of hot hydrogen above 200 GPa, *Nat. Mater.* **14**, 495 (2015).
- [18] See Supplemental Material at <http://link.aps.org/supplemental/10.1103/PhysRevResearch.5.033100> for the details of experimental methods, DAC techniques, example of pressure measurements at high PT conditions, all isothermal and isobaric plots for the vibron ν_1 model, and pressure-temperature dependencies for low-frequency Raman modes.
- [19] R. T. Howie, E. Gregoryanz, and A. F. Goncharov, Hydrogen (deuterium) vibron frequency as a pressure comparison gauge at multi-Mbar pressures, *J. Appl. Phys.* **114**, 073505 (2013).
- [20] Y. Akahama and H. Kawamura, Pressure calibration of diamond anvil Raman gauge to 410 GPa, *J. Phys.: Conf. Ser.* **215**, 012195 (2010).
- [21] H. Herchen and M. A. Cappelli, First-order Raman-spectrum of diamond at high-temperatures, *Phys. Rev. B* **43**, 11740 (1991).
- [22] B. J. Baer, W. J. Evans, and C. S. Yoo, Coherent Anti-Stokes Raman Spectroscopy of Highly Compressed Solid Deuterium at 300 K: Evidence for a New Phase and Implications for the Band Gap, *Phys. Rev. Lett.* **98**, 235503 (2007).
- [23] C. Ji, B. Li, W. Liu, J. S. Smith, A. Majumdar, W. Luo, R. Ahuja, J. Shu, J. Wang, S. Sinogeikin *et al.*, Ultrahigh-pressure isostructural electronic transitions in hydrogen, *Nature (London)* **573**, 558 (2019).
- [24] I. F. Silvera, The solid molecular hydrogens in the condensed phase: Fundamentals and static properties, *Rev. Mod. Phys.* **52**, 393 (1980).
- [25] R. J. Hemley, H. K. Mao, and J. F. Shu, Low-Frequency Vibrational Dynamics and Structure of Hydrogen at Megabar Pressures, *Phys. Rev. Lett.* **65**, 2670 (1990).
- [26] P. Dalladay-Simpson, R. T. Howie, and E. Gregoryanz, Evidence for a new phase of dense hydrogen

- above 325 gigapascals, *Nature (London)* **529**, 63 (2016).
- [27] R. J. Hemley, J. H. Eggert, and H. K. Mao, Low-frequency Raman-spectroscopy of deuterium to megabar pressures at 77–295 K, *Phys. Rev. B* **48**, 5779 (1993).
- [28] R. T. Howie, T. Scheler, C. L. Guillaume, and E. Gregoryanz, Proton tunneling in phase IV of hydrogen and deuterium, *Phys. Rev. B* **86**, 214104 (2012).
- [29] C. J. Pickard, M. Martinez-Canales, and R. J. Needs, Density functional theory study of phase IV of solid hydrogen, *Phys. Rev. B* **85**, 214114 (2012).
- [30] C. J. Pickard, M. Martinez-Canales, and R. J. Needs, Erratum: Density functional theory study of phase IV of solid hydrogen [Phys. Rev. B 85, 214114 (2012)], *Phys. Rev. B* **86**, 059902(E) (2012).
- [31] A. F. Goncharov, I. I. Mazin, J. H. Eggert, R. J. Hemley, and H. K. Mao, Invariant Points and Phase-Transitions in Deuterium at Megabar Pressures, *Phys. Rev. Lett.* **75**, 2514 (1995).
- [32] M. P. Surh, K. J. Runge, T. W. Barbee, E. L. Pollock, and C. Mailhot, Ab initio calculations for solid molecular hydrogen, *Phys. Rev. B* **55**, 11330 (1997).
- [33] A. Lagendijk, R. J. Wijngaarden, and I. F. Silvera, Roton-phonon mixing in solid hydrogen and deuterium, *Phys. Rev. B* **31**, 1352 (1985).
- [34] R. J. Wijngaarden, V. V. Goldman, and I. F. Silvera, Pressure dependence of the optical phonon in solid hydrogen and deuterium up to 230 kbar, *Phys. Rev. B* **27**, 5084 (1983).
- [35] M. I. Eremets, A. P. Drozdov, P. P. Kong, and H. Wang, Semimetallic molecular hydrogen at pressure above 350 GPa, *Nat. Phys.* **15**, 1246 (2019).
- [36] M. I. Eremets, I. A. Troyan, and A. P. Drozdov, Low temperature phase diagram of hydrogen at pressures up to 380 GPa. A possible metallic phase at 360 GPa and 200 K, *arXiv:1601.04479* (2016).
- [37] P. Loubeyre, F. Occelli, and R. LeToullec, Optical studies of solid hydrogen to 320 GPa and evidence for black hydrogen, *Nature (London)* **416**, 613 (2002).
- [38] H. Liu, L. Zhu, W. Cui, and Y. Ma, Room-temperature structures of solid hydrogen at high pressures, *J. Chem. Phys.* **137**, 074501 (2012).
- [39] C. Y. Zhang, C. Zhang, M. Chen, W. Kang, Z. Gu, J. Zhao, C. Liu, C. Sun, and P. Zhang, Finite-temperature infrared and Raman spectra of high-pressure hydrogen from first-principles molecular dynamics, *Phys. Rev. B* **98**, 144301 (2018).
- [40] A. F. Goncharov, J. S. Tse, H. Wang, J. Yang, V. V. Struzhkin, R. T. Howie, and E. Gregoryanz, Bonding, structures, and band gap closure of hydrogen at high pressures, *Phys. Rev. B* **87**, 024101 (2013).
- [41] H. Liu and Y. Ma, Proton or Deuteron Transfer in Phase IV of Solid Hydrogen and Deuterium, *Phys. Rev. Lett.* **110**, 025903 (2013).
- [42] J. M. McMahon, M. A. Morales, C. Pierleoni, and D. M. Ceperley, The properties of hydrogen and helium under extreme conditions, *Rev. Mod. Phys.* **84**, 1607 (2012).
- [43] A. F. Goncharov, I. Chuvashova, C. Ji, and H. K. Mao, Intermolecular coupling and fluxional behavior of hydrogen in phase IV, *Proc. Natl. Acad. Sci. USA* **116**, 25512 (2019).
- [44] J. M. McMahon and D. M. Ceperley, Ground-State Structures of Atomic Metallic Hydrogen, *Phys. Rev. Lett.* **106**, 165302 (2011).
- [45] G. Rillo, M. A. Morales, D. M. Ceperley, and C. Pierleoni, Coupled electron-ion Monte Carlo simulation of hydrogen molecular crystals, *J. Chem. Phys.* **148**, 102314 (2018).
- [46] I. B. Magdau and G. J. Ackland, Identification of high-pressure phases III and IV in hydrogen: Simulating Raman spectra using molecular dynamics, *Phys. Rev. B* **87**, 174110 (2013).
- [47] M. Borinaga *et al.*, Anharmonic enhancement of superconductivity in metallic molecular *Cmca*-4 hydrogen at high pressure: A first-principles study, *J. Phys.: Condens. Matter* **28**, 494001 (2016).
- [48] H. Y. Geng, H. X. Song, J. F. Li, and Q. Wu, High-pressure behavior of dense hydrogen up to 3.5 TPa from density functional theory calculations, *J. Appl. Phys.* **111**, 063510 (2012).
- [49] W. J. Nellis, A. C. Mitchell, P. C. McCandless, D. J. Erskine, and S. T. Weir, Electronic Energy Gap of Molecular Hydrogen from Electrical Conductivity Measurements at High Shock Pressures, *Phys. Rev. Lett.* **68**, 2937 (1992).
- [50] S. T. Weir, A. C. Mitchell, and W. J. Nellis, Metallization of Fluid Molecular Hydrogen at 140 GPa (1.4 Mbar), *Phys. Rev. Lett.* **76**, 1860 (1996).
- [51] M. Zaghoo, A. Salamat, and I. F. Silvera, Evidence of a first-order phase transition to metallic hydrogen, *Phys. Rev. B* **93**, 155128 (2016).
- [52] P. M. Celliers *et al.*, Insulator-metal transition in dense fluid deuterium, *Science* **361**, 677 (2018).
- [53] M. D. Knudson *et al.*, Direct observation of an abrupt insulator-to-metal transition in dense liquid deuterium, *Science* **348**, 1455 (2015).
- [54] S. Azadi, N. D. Drummond, and W. M. C. Foulkes, Nature of the metallization transition in solid hydrogen, *Phys. Rev. B* **95**, 035142 (2017).
- [55] K. A. Johnson and N. W. Ashcroft, Structure and bandgap closure in dense hydrogen, *Nature (London)* **403**, 632 (2000).
- [56] M. A. Morales, C. Pierleoni, E. Schwegler, and D. M. Ceperley, Evidence for a first-order liquid-liquid transition in high-pressure hydrogen from *ab initio* simulations, *Proc. Natl. Acad. Sci. USA* **107**, 12799 (2010).
- [57] C. Pierleoni, M. A. Morales, G. Rillo, M. Holzmann, and D. M. Ceperley, Liquid-liquid phase transition in hydrogen by coupled electron-ion Monte Carlo simulations, *Proc. Natl. Acad. Sci. USA* **113**, 4953 (2016).
- [58] P. I. C. Cooke, I. B. Magdau, and G. J. Ackland, Calculating the Raman signal beyond perturbation theory for a diatomic molecular crystal, *Comput. Mater. Sci.* **210**, 111400 (2022).